Published for SISSA by Springer

Received: December 21, 2022
Revised: May 12, 2023
Accepted: July 9, 2023
Published: July 31, 2023

Bubble nucleation and gravitational waves from holography in the probe approximation

Yidian Chen,[a] **Danning Li**[b] **and Mei Huang**[a]

[a] *School of Nuclear Science and Technology, University of Chinese Academy of Sciences, No.19(A) Yuquan Road, Shijingshan District, Beijing 100049, P.R. China*
[b] *Department of Physics and Siyuan Laboratory, Jinan University, 601 Huangpu Avenue West, Guangzhou 510632, P.R. China*

E-mail: chenyidian@ucas.ac.cn, lidanning@jnu.edu.cn, huangmei@ucas.ac.cn

Abstract: We investigate the bounce solution in the holographic dark-QCD and electroweak models with first-order phase transition. The strength parameter α, inverse duration time β/H and bubble wall velocity v_w in the gravitational wave power spectra are calculated by holographic bounce solution. We find the parameter α is about $\mathcal{O}(1)$ and β/H is about 10^4, which implies that the phase transition is fast and strong. The critical temperature, nucleation temperature and the temperature at the beginning time of the phase transition are close to each other in the holographic model. In addition, the velocity v_w is found to be less than the sound speed of the plasma $c_s = 1/\sqrt{3}$, which corresponds to the deflagration scenario. The gravitational wave signal from phase transitions is difficult to detect since the factor Υ suppresses the gravitational wave power spectrum. The GW signal can be detected only when the model is in the period of electroweak phase transition and with suitable parameters. Moreover, the primordial black hole is not favorable for formation due to the large parameter β/H and small velocity v_w.

Keywords: Holography and Hydrodynamics, Phase Transitions in the Early Universe, The Strong Coupling

ArXiv ePrint: 2212.06591

https://doi.org/10.1007/JHEP07(2023)225

Contents

JHEP07(2023)225

1 Introduction

Gravitational waves (GWs) are one of the great predictions of general relativity [1, 2], which exhibits an effect of the curvature of spacetime. In 2015, astronomy entered the multi-messenger era with the first observation of a gravitational wave event by LIGO [3]. Nowadays, more and more GW events or possible GW signals are discovered, as in refs. [4, 5], which also provide new instruments for understanding cosmology and astronomy deeply.

GWs come from the quadrupole moment radiation of the stress-energy tensor, which can be roughly classified into two categories, that is, cosmological and astronomical sources (see the reviews refs. [6–8]). The stochastic GW background generated by the first-order phase transition (FOPT) of the early universe is a significant cosmological source of GWs (see the reviews ref. [9]). Different from the transient GWs observed at present, the stochastic GW background comes from all directions rather than specific ones.

The detection experiments of GWs mainly include ground-based experiments, space-based experiments, pulsar timing arrays (PTA), and cosmic microwave background polarization, (see [10] for review). The ground-based experiments, such as LIGO [11], Virgo [12], Einstein Telescope (ET) [13], Cosmic Explorer (CE) [14], etc., mainly observe compact binary systems. The space-based experiments, such as Laser Interferometer Space Antenna (LISA) [15], Deci-Hertz Interferometer Gravitational wave Observatory (DECIGO) [16, 17], Big Bang Observer (BBO) [18], Taiji [19], Tianqin [20], etc., are more sensitive to the GWs from electroweak phase transition. The PTAs, such as the Parkes PTA (PPTA) [21], the European PTA (EPTA) [22], the North American Nanohertz Observatory for Gravitational Waves (NANOGrav) [23], the International PTA (IPTA) [24] and the Chinese PTA (CPTA), etc., are mainly sensitive to the GWs from phase transitions at the QCD scale.

The dynamic process of the FOPT is described by bubble dynamics. When the temperature of the system reaches the critical temperature T_c for the phase transition, it does not immediately enter the symmetric broken phase since the generation of true vacuum bubbles cause additional surface free energy, which increases the total free energy of the system. As the temperature decreases to the temperature at the beginning time of the phase transition $T(t_H)$, bubbles are more likely to be generated due to the increasing probability of thermal perturbation or quantum tunneling that crosses the free energy barrier. The temperature drops further to the nucleation temperature T_n, and about 64% of the space enters into the true vacuum. During this process, the bubble expands continuously since the internal pressure is greater than the false vacuum pressure and surface tension, and it may eventually reach the final velocity because of the friction of the plasma or accelerate to near the speed of light. Throughout the process, collisions of bubbles, acoustic modes of the plasma and turbulences of the magnetohydrodynamics all generate GWs and eventually contribute to the GW power spectra.

During the evolution of the universe, it may undergo various phase transitions, such as grand unification phase transition, electroweak phase transition (EWPT), and QCD phase transition. The FOPT is of interest since it is related to some physical processes such as baryogenesis, the seeds of intergalactic magnetic fields and the formation of primordial black holes. Unfortunately, the electroweak part of the standard model is crossover [25–27], while the Lattice QCD calculations indicate that the QCD phase transition of the three flavors is crossover at zero chemical potential and finite temperature [28, 29]. Of course, many new physical models beyond the Standard Model predict the FOPT, such as the two-Higgs doublet model [30–32], the left-right symmetric model [33], the technicolor model [34–36], etc. In addition, if there exists a dark or hidden QCD (dQCD), which is used to solve the dark matter puzzle [37–39], then the first-order phase transition at the QCD scale (dQCDPT) is still available.

The discovery of the anti-de Sitter/conformal field theory (AdS/CFT) correspondence [40–42] has provided a new way to solve strongly coupled field theory calculations. In the past two decades, holographic QCD has been widely studied both in top-down [43–45] and bottom-up models [46–52]. For beyond the standard model the technicolor model [53–58] and composite Higgs model [59–62] have been extended to the holographic framework.

The intensity of the GW signal is impacted by the strength of the phase transition, its duration time and the final velocity of the bubble wall. The calculations in weakly coupled quantum field theory suggest that the strength parameter α is roughly $\alpha \sim 0.01$ and the inverse of the duration time β/H is roughly $\beta/H \sim 100$ during EWPT, e.g. Refs. [33, 63]. As for the speed, one would expect that it is close to the speed of light c for enhancing the GW signal. These quantities are not sufficiently discussed and understood when the system is strongly coupled. The holographic principle provides new ways to explore the thermodynamic and kinetic properties of phase transitions with strong coupling. The bubble nucleation dynamics [64–75] and the GW power spectra [56, 76–81] are considered in the holographic model. The relation between the bubble velocity and the pressure difference of the true and false vacuum is investigated in refs. [66, 68, 75]. In refs. [72, 73], the profile of the fluid velocity is calculated inside and outside the bubble wall.

JHEP07(2023)225

The paper is organized as follows. The five-dimensional holographic dQCD and electroweak models are introduced in section 2. In section 3, the bounce solution and the thin-wall approximation are considered are obtained in the holographic model. Using the bounce solution, the bubble expansion and bubble wall velocity are obtained in section 4. In section 5, the stochastic GW power spectra generated by the strongly coupled FOPT are calculated. Finally, the conclusion and discussion are presented in section 6.

2 5d setup

In this section, we consider FOPT of dQCD or QCD-like electroweak theories, which corresponds to $\mathrm{SU}(N_f)_L \times \mathrm{SU}(N_f)_R$ flavor symmetry breaking to $\mathrm{SU}(N_f)_V$ subgroup. Here, only the scalar part of the flavor-brane is considered under the probe approximation, which has the following form [47, 82–84]

$$S = -\int d^5x\sqrt{-g}e^{-\Phi}\mathrm{Tr}[(D^M X)^\dagger(D_M X) + V_X(|X|)]. \tag{2.1}$$

Among this, Φ denotes the dilaton field and the complex scalar field X corresponds to the dark-quark condensation $\langle\bar{q}q\rangle$ or fermionic condensate of some theories beyond the Standard Model [85–92]. The symmetry of the model is spontaneously broken by the non-zero vacuum expectation value of the scalar field $X = \frac{\chi(z,x)}{\sqrt{2N_f}} I_{N_f}$, where I_{N_f} is the $N_f \times N_f$ identity matrix and χ depends not only on the fifth coordinate z but also on the four-dimensional space-time coordinates x^μ.

In this paper, the back-reaction of the dilaton field Φ and the scalar field X are not taken into account, so the background geometry remains the AdS_5-Schwarzchild black brane metric

$$ds^2 = \frac{L^2}{z^2}\left[-f(z)dt^2 + \frac{1}{f(z)}dz^2 + dx_i dx^i\right], \tag{2.2}$$

with the blackening factor $f(z) = 1 - \frac{z^4}{z_h^4}$ and the horizon z_h. For convenience, the AdS radius L is set to 1 in the following. The Hawking temperature of the system is

$$T = \frac{|f^{'}(z)|}{4\pi} = \frac{1}{\pi z_h}. \tag{2.3}$$

In order to realize the FOPT, the potential of the scalar field is considered to have the following form [82–84]

$$V(\chi) \equiv \mathrm{Tr}[V_X(|X|)] = \frac{M_5^2}{2}\chi^2 + \upsilon_3\chi^3 + \upsilon_4\chi^4 + \upsilon_6\chi^6, \tag{2.4}$$

where M_5^2 denotes the square of the five-dimensional mass, and υ_3, υ_4 and υ_6 are the cubic, quadratic and sextic terms coupling constants, respectively. According to the AdS/CFT dictionary, the five-dimensional mass of the scalar field X is $M_5^2 = (\Delta - p)(\Delta + p - 4) = -3$ by taking $p = 0$ and $\Delta = 3$ for dQCD. For the EW model, a large anomalous dimension $\gamma_m \simeq 1$ needs to be considered [93–98], so the five-dimensional mass is $M_5^2 = (\Delta - \gamma_m)(\Delta - \gamma_m - 4) = -4$ by taking $\Delta = 3$ and $\gamma_m = 1$. For simplicity, we do not consider all nonzero nonlinear

JHEP07(2023)225

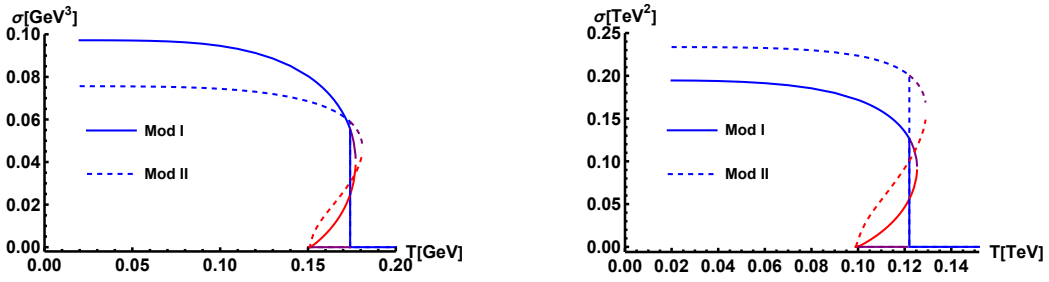

(a) (b)

Figure 1. The condensate σ as a function of temperature T. Panels (a) and (b) correspond to the dQCD and EW cases, respectively.

terms, but instead consider two special cases, i.e., $\upsilon_6 = 0$ (Model I) or $\upsilon_3 = 0$ (Model II). The correct chiral symmetry breaking in the chiral limit depends on the form of the dilaton field, which is chosen as in refs. [82, 83]

$$\Phi = -\mu_1 z^2 + (\mu_1 + \mu_0) z^2 \tanh(\mu_2 z^2), \tag{2.5}$$

where the μ_0, μ_1, and μ_2 parameters determine the behavior of the dilaton field in the IR and UV.

In this holographic model, five free parameters $[\mu_0, \mu_1, \mu_2, \upsilon_3, \upsilon_4]$ or $[\mu_0, \mu_1, \mu_2, \upsilon_4, \upsilon_6]$ are included. For the dQCD case, we choose $[\mu_0, \mu_1, \mu_2, \upsilon_3, \upsilon_4] = [(0.43\text{GeV})^2, (0.83\text{GeV})^2, (0.176\text{GeV})^2, -3, 8]$ (Model I) or $[\mu_0, \mu_1, \mu_2, \upsilon_4, \upsilon_6] = [(0.43\text{GeV})^2, (0.83\text{GeV})^2, (0.176\text{GeV})^2, -12, 100]$ (Model II) with the critical temperature of the phase transition $T_c \simeq 174\,\text{MeV}$, by referring to refs. [82–84]. For the EW case, $\mu_0 = \mu_2 = 0$ is chosen to simplify the model. It is worth noting that if $\Phi = -\mu_1 z^2$ is chosen, there is an additional massless scalar meson in the particle spectra, as in ref. [99]. For QCD, this is nonphysical. However, for the EW, this state can be interpreted as the Higgs boson, which obtains mass by interacting with other scalar fields. Therefore, for the EW case, the parameters are chosen as $[\mu_0, \mu_1, \mu_2, \upsilon_3, \upsilon_4] = [0, (0.28\text{TeV})^2, 0, -1.1, 3]$ (Model I) or $[\mu_0, \mu_1, \mu_2, \upsilon_4, \upsilon_6] = [0, (0.28\text{TeV})^2, 0, -1.8, 4]$ (Model II) with critical temperatures of $T_c \simeq 122\,\text{GeV}$. For the dQCD and EW cases, the parameters of Models I and II are listed in table 1. The Panels. (a) and (b) of figure 1 show the dQCD and technicolor condensate as a function of temperature, respectively. In fact, the specific values of these parameters do not affect the qualitative results in the following sections. In principle, the same approach can be used for symmetry breaking of other groups, simply by changing the representation of the group.

3 Bounce solution and thin-wall approximation

In this section, we will study the critical bubble of the FOPT in the holographic model, which will describe how the phase transition occurs and how long the phase transition lasts. The phase transition kinetics are characterized by nucleation temperature, latent heat, transition rate parameters, etc., which will determine the specific magnitude of the GW spectrum.

JHEP07(2023)225

Params	dQCD		EW	
	Mod. I	Mod. II	Mod. I	Mod. II
μ_0	$(0.43\text{GeV})^2$		0	
μ_1	$(0.83\text{GeV})^2$		$(0.28\text{TeV})^2$	
μ_2	$(0.176\text{GeV})^2$		0	
υ_3	-3	0	-1.1	0
υ_4	8	-12	3	-1.8
υ_6	0	100	0	4

Table 1. The parameters of Models I and II for dQCD and EW.

The kinetic process of the FOPT is described by the nucleation theory, in which the creation, expansion and fusion of bubbles transform the false vacuum χ_f into the true vacuum χ_t. The bubble nucleation is caused by quantum tunneling or thermal perturbation. At the critical temperature T_c, the true and false vacuums have the same free energy, and the phase transition is suppressed due to the surface free energy of the bubbles increasing the total free energy of the system. As the temperature decreases, the difference between the free energy of the true and false vacuum compensates for the surface free energy, and the bubble generation becomes more and more probable until the phase transition is completed.

The nucleation theory of relativistic systems was established by Coleman and Callan in the 1970s [100, 101]. Soon, Linde [102, 103] extended nucleation to the non-zero temperature situation. In addition, an effective field theory approach to nucleation theory was developed in ref. [104]. See ref. [105] for some reviews.

3.1 Bounce solution

In this subsection, we will construct bubble solutions in the holographic model. Considering the spherical symmetry of the bubble, the AdS-Schwarzchild metric is rewritten in spherical coordinates

$$ds^2 = \frac{1}{z^2}\left[-f(z)dt^2 + \frac{1}{f(z)}dz^2 + dr^2 + r^2 d\theta^2 + r^2\sin^2\theta d\varphi^2\right], \quad (0 \le r \le R) \tag{3.1}$$

with azimuth φ, zenith angle θ and the edge R. Then, the equations of motion of the scalar field X can be obtained from action (2.1)

$$\partial_r^2\chi(z,r) + \frac{2\partial_r\chi(z,r)}{r} + f(z)\partial_z^2\chi(z,r) + \left(f'(z) - f(z)\Phi'(z) - \frac{3f(z)}{z}\right)\partial_z\chi(z,r) - \frac{\partial_\chi V(\chi)}{z^2} = 0. \tag{3.2}$$

Coleman and Callan [100, 101] proposed that the critical bubble is described by the bounce solution in quantum nucleation theory. The solution requires the following boundary conditions

$$\lim_{r\to\infty}\chi(z,r) = \chi_f, \tag{3.3}$$

$$\left.\frac{d\chi(z,r)}{dr}\right|_{r=0} = 0. \tag{3.4}$$

The Chebyshev spectral method (its details can be described in ref. [106]) is applied to solve the eq. (3.2) with boundary conditions eq. (3.3) and eq. (3.4). Combined with the Newton's iteration method, the solution can be obtained. For the fifth dimensional direction, the expansion of the scalar field χ at the conformal boundary has the following form

$$\chi|_{z\to 0} = m_q\zeta z + \ldots + \frac{\sigma}{\zeta}z^3 + \ldots \quad \text{(dQCD)}, \tag{3.5}$$

$$= \sigma z^2 + \ldots \quad \text{(EW)}, \tag{3.6}$$

with the dark-quark current mass m_q, the condensate σ and constant $\zeta = \frac{\sqrt{3}}{2\pi}$ [107]. Since the FOPT is considered, it is convenient to set the current mass m_q to 0. At the IR boundary, the natural boundary conditions are selected such that the field does not diverge at the IR. Under saddle point approximation, the tunneling rate of the stochastically generated bubbles is

$$\Gamma(T) = A(T)e^{-\frac{S_b}{T}}, \tag{3.7}$$

where S_b is the Euclidean action evaluated on the bounce solution and the factor is $A = T^4(\frac{S_b}{2\pi T})^{3/2}$ [102, 103]. According to the holographic principle, the partition function has the equivalence $\mathcal{Z}_{\rm QFT} \simeq \mathcal{Z}_{\rm Gra}$, so the action S_b can be calculated by the gravitational part $S_b \simeq S_5$. The Euclidean action of the bounce solution has the following form

$$S_b \simeq S_5 = 4\pi \int_0^R dr \int_0^{z_h} dz\sqrt{-g}e^{-\Phi(z)}\left(-\frac{\upsilon_3}{2}\chi^3 - \upsilon_4\chi^4 - 2\upsilon_6\chi^6\right). \tag{3.8}$$

By solving the equation of motion eq. (3.2) with the boundary conditions eqs. (3.3)–(3.6), we can obtain the bounce solution in the holographic model. For simplicity, we focus on the case of the dQCD phase transition with $\upsilon_3 \neq 0$ (Model I). For other parameter values or holographic EW models, the qualitative conclusions do not change. The panel (a) of figure 2 shows the scalar field χ as a function of the fifth dimensional coordinate z and the radial coordinate r at a temperature of 172 MeV. It can be seen that the scalar field χ has a nontrivial structure as a function of z when the radial r is small, while the profile of χ varies continuously to the trivial solution as r tends to the edge R.

The panel (b) of figure 2 represents the condensation as a function of radial r at different temperatures. It can be seen that the size of the critical bubble diminishes with decreasing temperature. As the temperature decreases, the free energy barrier between the true and false vacuums is reduced, and small-size bubbles are more likely to form. It should be noted that the condensation values at the center of the bubble do not reach the equilibrium values when $T \lesssim 170$ MeV. This can be interpreted as the fact that at that temperature, the bubbles are composed mainly of bubble walls, as can be seen from panel (b) of figure 2. The true vacuum is revealed inside the bubble when $T \gtrsim 170$ MeV.

3.2 Thin-wall approximation

In the previous subsection, we have obtained the bounce solution. By analyzing the properties of the holographic bounce solution, the characteristics of the strong FOPT can be understood qualitatively, which helps to understand its GW power spectrum. We know

JHEP07(2023)225

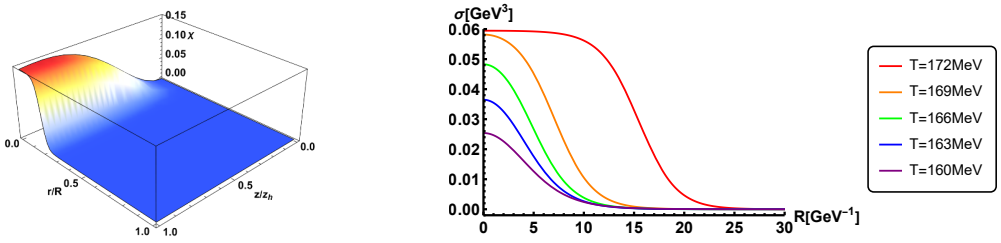

(a) (b)

Figure 2. The panel (a) represents the bounce solution of the scalar field χ_b as a function of the fifth dimensional coordinate z and the radial coordinate r. The panel (b) indicates the condensate σ as a function of the radial coordinate r at different temperatures.

that there are three important characteristic temperatures during the dynamical FOPT that exhibit the details of the phase transition and are finally reflected in the GW. The first one is the critical temperature T_c of the phase transition, i.e., the temperature at which the free energy has a degenerate minimum. The rest are the temperature at the beginning time of the phase transition $T(t_H)$ and nucleation temperature T_n, which represent the temperature of beginning nucleation and ending of phase transition, respectively. The temperature $T(t_H)$ and T_n are mainly determined by the profile of the Euclidean action $\frac{S_b}{T}$ of bounce solution with temperature. In addition, the bubble wall thickness and bubble radius can be obtained from the bounce solution. In this section, we analyze the holographic behavior of the bounce solution with temperature. It should be noted that we only show the dQCDPT with $v_3 \neq 0$ (Model I). For $v_6 \neq 0$ (Model II) or EWPT, the numerical results change slightly and the conclusions in the following still apply.

From eq. (3.8) we can calculate the Euclidean action $\frac{S_b}{T}$. Figure 3 shows the on-shell action $\frac{S_b}{T}$ as a function of $\frac{T}{T_c}$ calculated by the bounce solution. It can be seen from the figure that the value of the action decreases rapidly as the temperature decreases, and at about $\frac{T}{T_c} \sim 0.99$, i.e., at a temperature of about 172 MeV, $\frac{S_b}{T}$ drops to 30. The temperature at the beginning time of the phase transition $T(t_H)$ can be given by relation $\frac{S_b(T_n)}{T_n} \sim 180$ for dQCDPT ($\frac{S_b(T_n)}{T_n} \sim 140$ for EWPT) (a more rigorous definition is shown in the next section). Therefore, the temperature at the beginning time of the phase transition is very close to the critical temperature $T_c \simeq T(t_H)$. Furthermore, at low temperatures, the action does not have a local minimum. Also, since the nucleation probability Γ is proportional to the action, it can be seen that bubbles are created rapidly and abundantly as the temperature decreases. Consequently, it is reasonable to suppose that the nucleation temperature is close to the temperature at the beginning time of the phase transition $T(t_H) \simeq T_n$. As shown above, the three characteristic temperatures have relation $T_c \simeq T(t_H) \simeq T_n$, which corresponds to the strongly supercooling case [108].

We use hyperbolic tangent function interpolation condensation as a function of the radial r, shown following

$$\sigma(T,r) = \frac{\sigma_0(T)}{2}\left[-\tanh\left(\frac{r - R_w(T)}{L_w(T)}\right) + 1\right], \tag{3.9}$$

JHEP07(2023)225

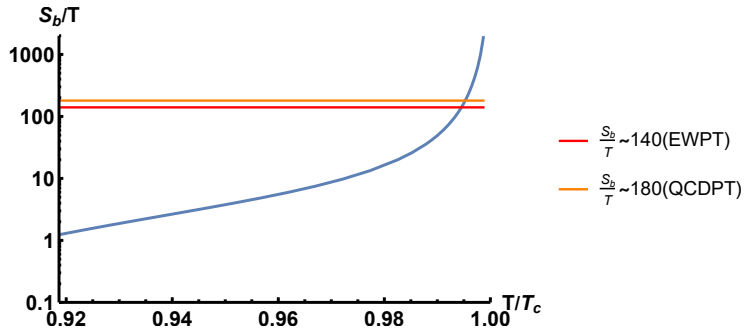

Figure 3. The Euclidean action $\frac{S_b}{T}$ as a function of temperature.

where σ_0 is the condensation value at the center, R_w denotes the radius of the bubble, and L_w represents the thickness of the bubble wall. Unlike the previous section, these quantities are independent of time since the critical bubbles do not evolve with time. Figure 4 displays the condensation σ_0, radius R_w, and thickness L_w as functions of temperature. As seen in panel (a), the condensation at the center increases with increasing temperature at $T \lesssim 0.975T_c \sim 170\text{MeV}$ and has the opposite behavior at $T \gtrsim 0.975T_c$. Two factors with opposite effects influence this behavior. As can be seen in figure 1, the condensation value decreases continuously with increasing temperature; in contrast, as in figure 2, the critical bubble is larger at higher temperatures, which favors the generation of a true vacuum at the center. For the bubble radius R_w, panel (b) shows that the critical radius varies slightly at temperature $T \lesssim 0.98T_c \sim 171\text{MeV}$. However, at temperature $T \gtrsim 0.98T_c$, the critical radius of the bubble increases rapidly, which is not favorable for bubble generation. In contrast to the behavior of the bubble radius, the bubble wall thickness essentially does not vary with temperature. And the thickness changes slightly at low temperature $T \lesssim 0.94T_c \sim 164\text{MeV}$. This is because the hyperbolic function fitting is not a good choice at this time.

From the previous discussion, it is clear that in this holographic model, the FOPT is strongly supercooled. As in ref. [108], the thin-wall approximation can be applied in this case. Under this approximation, many physical quantities, such as latent heat, duration time of phase transition and surface tension of bubble, have simpler forms and can be obtained more easily. In this section, we estimate the surface tension and the parameters α and β/H using the Euclidean action obtained previously. Among them, the parameters α and β/H are very important for the GW power spectrum.

From refs. [108–110], the parameter α is

$$\alpha \simeq \frac{15}{2\pi^2} \frac{L_c}{g_*(T_c)T_c^4}, \tag{3.10}$$

where g_* is the relativistic degree of freedom of the system and L_c is the latent heat of phase transition. For the degree of freedom g_*, it relies on the complete theory, including the standard model and the holographic model. In this paper, the degrees of freedom of the holographic part are considered to be comparable to that of the Standard Model, and thus g_* has the following estimate. For dQCDPT (EWPT), the degrees of freedom can be

JHEP07(2023)225

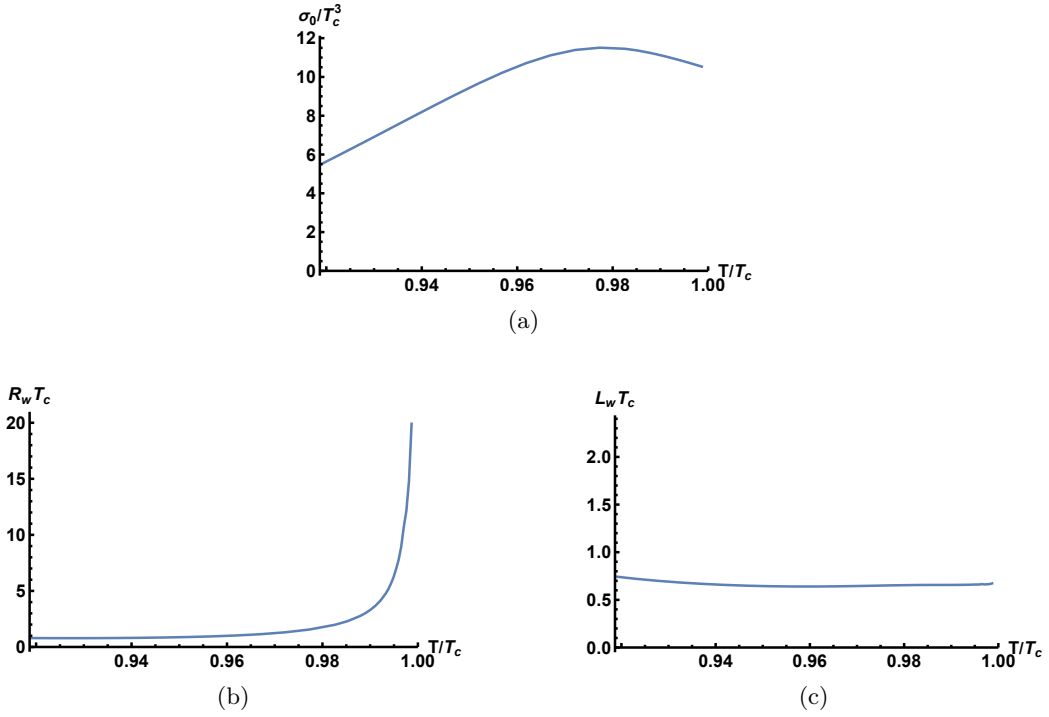

Figure 4. The panels (a), (b) and (c) show the condensation value at the center σ_0, the bubble radius R_w and the bubble wall thickness L_w as functions of the temperature, respectively.

approximated as $g_* \simeq 20$ ($g_* \simeq 200$). Under the thin-wall approximation, the latent heat has the following form

$$L_c = -T\frac{\partial \Delta V_{\text{eff}}(\langle\phi\rangle_T, T)}{\partial T}\bigg|_{T=T_c} = T\frac{\partial \Delta F(\langle\phi\rangle_T, T)}{\partial T}\bigg|_{T=T_c}, \tag{3.11}$$

with difference of the free energy ΔF. The calculation of the free energy F can be found in refs. [82, 83]. Within the approximation, the three-dimensional Euclidean action S_b can be divided into two parts, as follows

$$S_b(T) = -\frac{4\pi}{3}R_w(T)\varepsilon(T) + 4\pi R_w(T)^2\sigma_w(T), \tag{3.12}$$

with the $\varepsilon(T) = \Delta V_{\text{eff}}(\langle\phi\rangle_T, T)$ and surface tension σ_w of the bubble wall. From the above equation, it can be seen that the energy of the critical bubble consists of the vacuum energy inside the bubble and the surface energy of the bubble wall. With the bubble radius previously calculated, the surface tension can be obtained as shown in figure 5. For the low-temperature region in the figure, the result is not reliable because the thin-wall approximation no longer applies.

Also from ref. [108], the inverse of duration time β/H of the phase transition is given as

$$\frac{\beta}{H} = \left(\frac{3}{4\pi}\frac{T_c L_c^2}{\sigma_w(T_c)^3}\right)^{1/2}\left(\frac{S_b(T_n)}{T_n}\right)^{3/2}, \tag{3.13}$$

JHEP07(2023)225

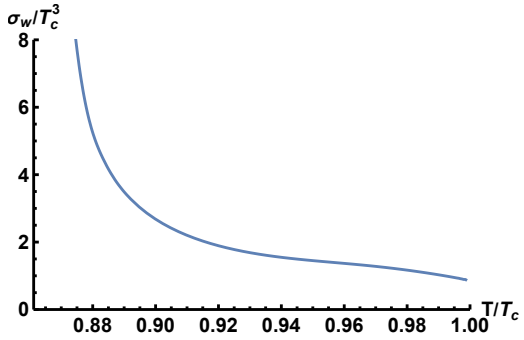

Figure 5. The surface tension σ_w of the bubble wall as a function of temperature.

Thin-wall approx	dQCDPT	EWPT
α	2-3	0.2-0.3
β/H	30000-60000	6000-20000

Table 2. The parameters α and β/H estimated by the thin-wall approximation during dQCDPT and EWPT.

with the nucleation temperature T_n. It should be noted that the above equation can only be applied under the thin-walled approximation, and the definition of β/H for the general case can be found in section 5. With the above definitions and the relation $T_c \simeq T(t_H) \simeq T_n$, the final results of parameters α and β/H are shown in table 2. From the table, we can find that for dQCDPT, the parameter α is greater than 1, about 2–3, which is strongly FOPT case, and the parameter β/H is large, which means that the phase transition ends rapidly. For EWPT, the strength parameter α is less than 1, while the inverse of the duration time remains large, which means that the phase transition is sufficiently fast, that is, the so-called weakly supercooled FOPT.

4 Bubble expansion and bubble wall velocity

When a large enough bubble is created in the plasma, it expands, collides with each other and eventually transforms the false vacuum into a true vacuum. During this process, some physical phenomena such as baryogenesis, GW generation, and primordial black hole formation will happen. It can be expected that the velocity of the bubble wall has an impact on the final signal. For the GW power spectrum, numerical simulations indicate that faster bubble wall velocity enhances the signal intensity [111].

The velocity of the bubble wall in the plasma is governed by hydrodynamics and particle interactions. The way bubbles expand is divided into deflagration, detonation, hybrid and runaway cases [109], which influence the GW spectra through bubble collisions and interactions with the hydrodynamics. In order to understand the details of FOPT more accurately, many methods have been used to calculate the bubble wall velocity. As in refs. [112–115], the local equilibrium hydrodynamic equations are applied to obtain the velocity. More generally, considering the effect of out of equilibrium, people need to

JHEP07(2023)225

solve the distribution function by the Boltzmann equation, which allows to obtain the velocity containing the backreaction [116–124]. In addition, the holographic method is also applied to the calculation of bubble wall velocity. In refs. [66–68, 72, 73, 75], applying the gauge/gravity duality, the bubble velocity is calculated for strongly coupled hydrodynamics.

In this letter, the probe approximation is considered, i.e., we only account for the obstruction from the plasma fluid without the backaction. To investigate the real-time evolution, we transform the framework to the ingoing Eddington-Finkelstein coordinate, then the metric becomes

$$ds^2 = \frac{1}{z^2}[-f(z)dt^2 - 2dtdz + dr^2 + r^2 d\theta^2 + r^2 \sin^2\theta d\varphi^2]. \tag{4.1}$$

Under the coordinate transformation, the scalar field χ is invariant, and its equation of motion becomes as follows

$$\partial_r^2\chi(t,z,r) + \frac{2\partial_r\chi(t,z,r)}{r} + f(z)\partial_z^2\chi(t,z,r) + \left(f'(z) - f(z)\Phi'(z) - \frac{3f(z)}{z}\right)\partial_z\chi(t,z,r)$$
$$- \frac{\partial_\chi V(\chi)}{z^2} + \left(\frac{3}{z} + \Phi'(z)\right)\partial_t\chi(t,z,r) - 2\partial_t\partial_z\chi(t,z,r) = 0. \tag{4.2}$$

In order to solve eq. (4.2), the equation requires suitable boundary conditions and initial condition. We choose the following boundary conditions at the center and edge

$$\partial_t\partial_r\chi|_{r=0} = \partial_t\partial_r\chi|_{r=R} = 0. \tag{4.3}$$

This means that the smoothness of the bubbles is ensured at the center and the edge. Of course, it is also possible to choose $\partial_t\chi|_{r=R} = 0$ at the edge, i.e., a false vacuum at the far distance all the time. We find that there is almost no difference between the two choices when the radial dimensions are large enough. It can be foreseen that the choice of this paper is more reasonable when the space contains more than one bubble. At the conformal boundary, we have

$$\partial_t\partial_z\chi|_{z=0} = 0. \tag{4.4}$$

This corresponds to the fact that the current mass is fixed and its does not vary with time. The numerical strategies for solving eq. (4.2) with boundary conditions eq. (4.3) and (4.4) are as follows. For the spatial z and r directions, the Chebyshev spectral method is applied, while the explicit fourth-order Runge-Kutta method is employed for the time evolution.

For the initial condition, we consider adding a perturbation $\delta\chi$ to the bounce solution of the scalar field χ_b. Because the meaning of the bounce solution is the critical bubble solution, i.e., any bubble larger than it will expand, and smaller than it will shrink. Since the bounce solution χ_b does not vary with time, the selection of the perturbation is important, which will determine whether the bubble expands or shrinks. Therefore, the perturbation $\delta\chi$ is not completely random, but is controlled to be positive or negative. In this paper, we choose the perturbation as follows

$$\delta\chi(z,r) = \mathcal{A}\,\chi_t(z)\{\exp[(r-r_0)^2] + 1\}^{-1}, \tag{4.5}$$

where $\mathcal{A}$ is a constant that is small enough, χ_t is the true vacuum solution at that temperature, and r_0 is an arbitrary number.

JHEP07(2023)225

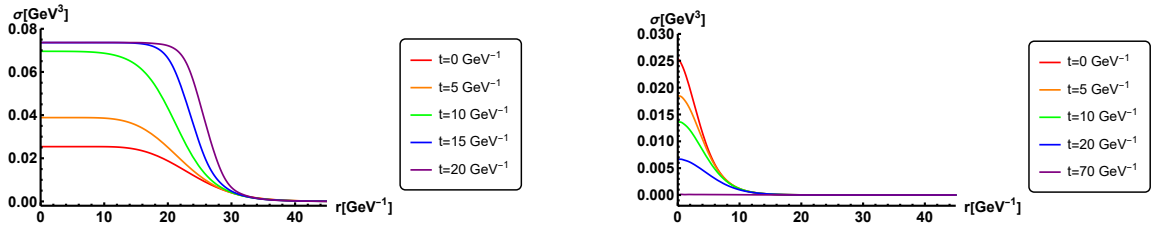

(a) (b)

Figure 6. The panels (a) and (b) show the profiles of the bubbles at different times with $T = 160\,\text{MeV}$ when positive and negative perturbations are added, respectively.

The panels (a) and (b) of figure 6 show the evolution of the bubble with time at $T = 160\,\text{MeV}$ when positive and negative perturbations are added, respectively. As seen in panel (a), when positive perturbation is added, the bubble goes through two steps. First the condensation value at the center of the bubble keeps growing until the true vacuum. After that, the structure of the bubble wall stabilizes and gradually expands outward. At times less than about $t \simeq 15\text{GeV}^{-1}$, the bubble is still in the first step, and when the time is greater than 15 GeV^{-1} the bubble enters the second step. If the temperature is $170\text{MeV} \lesssim T \lesssim 174\text{MeV}$, then the first step of bubble expansion does not occur. Of course, the exact timing of the distinction between the two steps is related to the amplitude of the perturbation, which is roughly equal in magnitude when the perturbation is small enough. The panel (b) displays the bubble shrinking with negative perturbation. As can be seen in the panel, the condensation value at the center of the bubble gradually decreases until the system completely returns to the false vacuum at $t \simeq 70\text{GeV}^{-1}$. The time of the bubble shrinking process is roughly comparable to the time of the first step of expansion, for bubbles that are neither too large nor too small.

To obtain the bubble wall velocity, we used the function $\sigma(r) = \frac{\sigma_0(t)}{2}[-\tanh(\frac{r(t)-r_w(t)}{l_w(t)})+1]$ to fit the profile of the condensation. Here, σ_0 is the condensation value at the center, r_w denotes the radius of the bubble, and l_w represents the thickness of the bubble wall. Figure 7 shows the numerical and fitting results. The red and green lines in the figure correspond to the condensation reaching and not reaching the true vacuum at the center, respectively. It can be seen that the function fits the numerical results quite well except at the edges of the bubble walls. Therefore, we can define the velocity of the bubble wall by $v(t) = dr_w(t)/dt$. The panel (a) of figure 8 exhibits the bubble wall velocity as a function of time at a temperature of 160 MeV. It can be seen that the velocity gradually increases with time, while the acceleration gradually decreases. The velocity reaches its final velocity about $0.32\,c$ when the time reaches about $t \simeq 500\text{GeV}^{-1}$. As for the relaxation time for the bubble to reach its final velocity, it depends on the strength of the perturbation. Numerical calculations show that the relaxation times with different perturbations are roughly equivalent. Note that the velocity is not well defined at time $t \lesssim 20\text{GeV}^{-1}$. This is because the bubble is still in the first step during this time and the wall configuration is changing and therefore not shown in the panel.

The final velocity of the bubble wall v_w is defined as $v_w = \lim_{t\to\infty} v(t)$. The panel (b) of figure 8 shows the final velocity of the bubble wall as a function of the pressure difference

JHEP07(2023)225

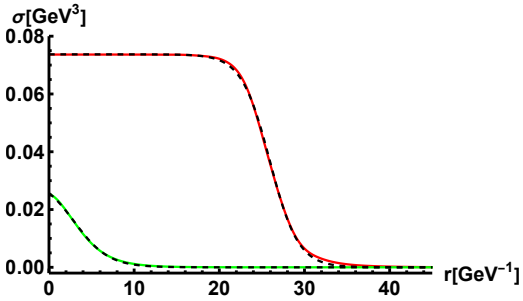

Figure 7. The condensate as a function of radial r, where the solid line is the numerical solution and the dashed line represents the fitting results of the hyperbolic tangent function. The red and green lines in the figure correspond to the condensation reaching and not reaching the true vacuum at the center, respectively.

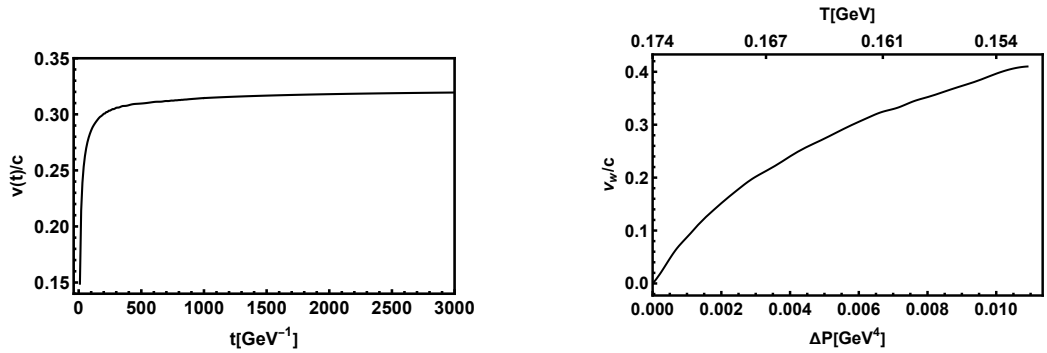

(a) (b)

Figure 8. The panel (a) shows the bubble wall velocity as a function of time. The panel (b) shows the final velocity of the bubble wall as a function of the pressure difference ΔP between the inside and outside or the temperature T.

ΔP between the inside and outside or the temperature T. According to the holographic principle, the pressure can be obtained from the free energy $F = -P$, as in refs. [82, 83]. At low temperatures, the final velocity is approximately linear with respect to the pressure difference, while at temperatures close to the critical temperature, their relation exhibits nonlinear behavior. In ref. [75], the relation between velocity and pressure difference has a nonlinear behavior. Although, the method used in ref. [75] is different from the one used in this paper, the behavior exhibited is very similar. It can be seen from the panel that even if the temperature drops to 154 MeV, the final velocity still does not exceed sound speed $c_s = 1/\sqrt{3}$ of the plasma, which corresponds to the deflagration case. This is in agreement with the results of refs. [66, 67, 72, 75]. It is reasonable to speculate that in the bottom-up holographic model, the final velocity is always limited to the deflagrations region because the system contains a holographic dissipation mechanism [125]. While in ref. [68], the Dp brane system can achieve bubble wall velocities close to the speed of light. Whether detonation and hybrid cases can be implemented in the bottom-up holographic model is still an open question.

JHEP07(2023)225

5 Stochastic gravitational waves

When the system reaches the temperature at the beginning time of the phase transition, bubbles will be created, and they will collide and merge together in the plasma. Then the false vacuum will be transformed into the true vacuum. In this process, part of the system's energy is eventually converted into GW radiation. Within the linear approximation, the total GW power spectra can be written as

$$h^2\Omega_{\rm GW} \simeq h^2\Omega_{\rm coll} + h^2\Omega_{\rm sw} + h^2\Omega_{\rm turb}, \tag{5.1}$$

where $\Omega_{\rm coll}$ comes from bubble collisions [109, 126–134], $\Omega_{\rm sw}$ from acoustic waves in the plasma after the collision [110, 135–138], and $\Omega_{\rm turb}$ from magnetohydrodynamic turbulence in the plasma [139–146].

In the previous section we have found that for the holographic model, the final velocity of the bubble wall is less than the speed of sound, i.e., the non-runaway case. According to refs. [109, 111, 129, 147–149], the GWs generated by collisions in the non-runaway case can be neglected with respect to acoustic waves and magnetohydrodynamic turbulence. Therefore, the total power spectrum is approximated to

$$h^2\Omega_{\rm GW} \simeq h^2\Omega_{\rm sw} + h^2\Omega_{\rm turb}. \tag{5.2}$$

From numerical simulations [110], the power spectrum from sound waves has the form of

$$h^2\Omega_{\rm sw}(f) = 2.65\times10^{-6}\left(\frac{H}{\beta}\right)\left(\frac{\kappa_s\alpha}{1+\alpha}\right)^2\left(\frac{100}{g_*}\right)^{\frac{1}{3}} v_w S_{\rm sw}(f)\Upsilon, \tag{5.3}$$

$$S_{\rm sw}(f) = (f/f_{\rm sw})^3\left(\frac{7}{4+3(f/f_{\rm sw})^2}\right)^{7/2}, \tag{5.4}$$

$$f_{\rm sw} = 1.9\times10^{-2}{\rm mHz}\frac{1}{v_w}\left(\frac{\beta}{H}\right)\left(\frac{T_n}{100{\rm GeV}}\right)\left(\frac{g_*}{100}\right)^{\frac{1}{6}}, \tag{5.5}$$

where the factor κ_s represents the ratio of vacuum energy transformed into bulk motion. The specific form of the factor κ_s depends on the bubble wall velocity and has the following form in the limits of large and small velocities

$$\kappa_s \simeq \begin{cases} \alpha\left(0.73+0.083\sqrt{\alpha}+\alpha\right)^{-1}, & v_w\sim 1, \\ v_w^{6/5}6.9\alpha\left(1.36-0.037\sqrt{\alpha}+\alpha\right)^{-1}, & v_w \lesssim 0.1. \end{cases} \tag{5.6}$$

From the table 2, it is obtained that the velocity is about $v_w \sim 0.1$, since the phase transition of the holographic model is supercooled. Therefore, in this paper, the expression for the factor κ_s is

$$\kappa_s = v_w^{6/5}6.9\alpha\left(1.36-0.037\sqrt{\alpha}+\alpha\right)^{-1}. \tag{5.7}$$

It should be noted that the power spectrum from sound waves in ref. [150] contains a suppression factor Υ. Although it is not known whether this suppression factor is applicable

JHEP07(2023)225

with $\alpha \sim \mathcal{O}(1)$, it provides a strong suppression compared to previous estimates [138, 151]. Therefore, the suppression factor Υ from ref. [150] is considered in this paper as

$$\Upsilon = 1 - \left[1 + \frac{8\pi^{\frac{1}{3}}}{\sqrt{3}} v_w \frac{H}{\beta} \left(\frac{\kappa_s \alpha}{\alpha + 1}\right)^{-\frac{1}{2}}\right]^{-\frac{1}{2}}. \tag{5.8}$$

It is worth noting that the suppression effect mentioned in ref. [149] is not taken into account in the suppression factor Υ. The reference points out that for deflagrations in strong phase transitions, the GW energy density is further suppressed due to the initial kinetic energy suppression as re-heats. For $\alpha \sim \mathcal{O}(1)$ and $v_w \sim 0.2$, the GW signal can be suppressed by a factor of 10^{-3}. The signal is further decreased if the kinetic suppression effect from ref. [149] is also included.

Since the numerical simulation of turbulence is very challenging, little is known about the GW generated by turbulence. To estimate the contribution of the turbulent component, one needs to know the ratio of the kinetic energy converted into vortical motion during the phase transition phase, which was estimated in refs. [110, 138]. In addition, ref. [149] found that vortical motion is more efficiently generated if the phase transition is deflagration with large α, i.e., the case of the holographic model. Also, refs. [152, 153] had performed numerical simulations, and refs. [132, 142, 154] had modeled to investigate. Due to the complexity of turbulence, the contribution from the turbulence is dropped in this paper to make a conservative estimate.

In the GW power spectrum, the parameters α and β/H are important, which represent the vacuum energy release and duration time of the phase transition, respectively. The parameter α is defined as

$$\alpha \equiv \frac{1}{\rho_{\rm rad}} \left(\Delta V_{\rm eff} - \frac{T}{4} \frac{\partial \Delta V_{\rm eff}}{\partial T}\right)\Big|_{T=T_n} = -\frac{1}{\rho_{\rm rad}} \left(\Delta F - \frac{T}{4} \frac{\partial \Delta F}{\partial T}\right)\Big|_{T=T_n}, \tag{5.9}$$

with radiation energy density

$$\rho_{\rm rad} = g_* \frac{\pi^2}{30} T^4. \tag{5.10}$$

The inverse of the duration time is defined as

$$\frac{\beta}{H} \equiv T \frac{d}{dT} \left(\frac{S_b}{T}\right)\Big|_{T=T_n}. \tag{5.11}$$

The definitions of the other two characteristic temperatures of the phase transition, i.e., temperature at the beginning time of the phase transition $T(t_H)$ and nucleation temperature T_n, are shown below. The temperature at the beginning time of the phase transition is defined as one bubble per unit Hubble volume and is written as

$$N(T_n) = \int_{T_n}^{T_c} \frac{\mathrm{d}T}{T} \frac{\Gamma(T)}{H(T)^4} = 1, \tag{5.12}$$

where the nucleation rate $\Gamma(T)$ is given in eq. (3.7) and the Hubble parameter $H(T)$ is

$$H(T) = \sqrt{\frac{\rho_{\rm rad} + \rho_{\rm vac}}{3M_{\rm pl}^2}}, \tag{5.13}$$

JHEP07(2023)225

with reduced Planck mass $M_{\rm pl} = 2.435{\cdot}10^{18}$ GeV. Referring to refs. [155–157], the probability of a false vacuum is defined as

$$P(T) = e^{-I(T)}, \tag{5.14}$$

with

$$I(T) = \frac{4\pi}{3}\int_T^{T_c} \mathrm{d}T' \frac{\Gamma(T')}{H(T')T'^4}\left(\int_T^{T'} \mathrm{d}T'' \frac{v_w(T'')}{H(T'')}\right)^3. \tag{5.15}$$

The nucleation temperature is defined as $I(T_n) \simeq 1$, which is the temperature when the probability of false vacuum is about $P(T_n) \simeq 1/e$.

The table 3 shows the quantities related to the phase transition in different holographic models. Here, the velocity v_w is selected at the nucleation temperature T_n. Compare to table I, we can see that the rigorous results are very close to that of thin-wall approximation. This further verifies the reliability of the approximation in the holographic model. It should be noted that the strength parameter α of dQCDPT is greater than 1, which would be a strongly supercooled FOPT. For EWPT, FOPT is weakly supercooled. It is worth noting that although dQCDPT is strongly supercooled, its properties are very similar to those of the EWPT and there are no minimum values of the weights S_b/T as mentioned in the ref. [108]. Furthermore, for parameters α and β/H, we find an inverse relation between them, which is similar to that of ref. [108]. For Models I and II, we found that Model II ($\upsilon_6 \neq 0$) has lower nucleation temperature and larger bubble wall velocity, which favors a bigger GW signal.

From table 3, we also find that the results of the holographic model differ significantly from those of the traditional calculations in perturbative quantum field theory. Moreover, the strength of the phase transition is greater than 0.1 for both color brane [56] and flavor brane in the holographic model. For the parameter β/H, perturbative field theory calculations show that it is generally not larger than 1000 [33, 63]. But for the holographic model, the parameter β/H is larger than 5000 during dQCDPT or EWPT. This means that the duration time of the strongly coupled phase transition is shorter compared to the weakly coupled case. Also, in ref. [81], the β/H obtained from the holographic model is about $10^4 - 10^5$. As for the bubble wall velocity, one would expect it to be close to the speed of light c. Unfortunately, the holographic results suggest that the bubble wall velocity is smaller than the sound speed of the plasma.

The GW power spectra of dQCDPT and EWPT for different holographic models are exhibited in figure 9. Due to the large value of β/H, the peak frequency of GW is larger compared to the results of perturbative quantum field theory, causing a right shift in the sensitive frequency interval of GW. For the holographic model of dQCDPT, the peak frequency is about 0.01 Hz. In addition, since the bubble wall velocity v_w is much less than the speed of light c and the significant suppression effect of the factor Υ, the GW signal $h^2\Omega$ can only reach about $10^{-18} - 10^{-19}$. For both Model I and Model II, it is not yet detectable by any experiment today. For EWPT, the peak frequency is around $1 - 10$ Hz, when the GW spectrum $h^2\Omega$ reaches about $10^{-17} - 10^{-20}$. For Model I, the GW signal is not detectable by any experiment. For Model II, it can be detected by Ultimate-DECIGO if the parameters are suitably modified.

JHEP07(2023)225

	dQCDPT		EWPT	
Model	I ($v_3 \neq 0$)	II ($v_6 \neq 0$)	I ($v_3 \neq 0$)	II ($v_6 \neq 0$)
g_*	10		100	
α	2.440	3.071	0.119	0.381
β/H	41151	23273	17198	7238
v_w	0.027	0.041	0.063	0.125
T_c[GeV]	0.1741		122.1	
$T(t_H)$[GeV]	0.1733	0.1712	120.7	118.1
T_n[GeV]	0.1732	0.1702	120.4	117.6

Table 3. The critical temperature T_c, temperature at the beginning time of the phase transition $T(t_H)$, nucleation temperature T_n of phase transition, parameters α, β/H, and bubble wall velocity v_w in different holographic models.

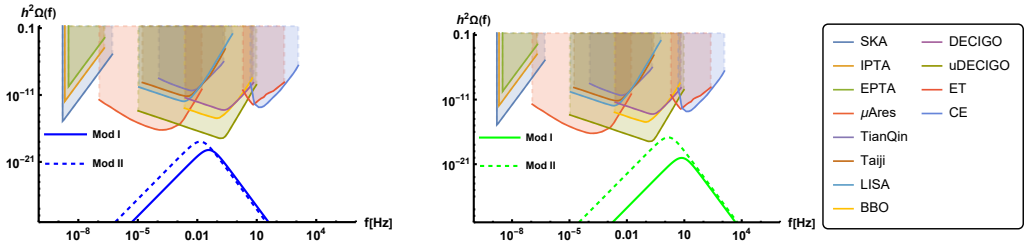

(a) (b)

Figure 9. The GW power spectra in different holographic models, where the blue (a) and green (b) lines represent dQCDPT and EWPT, respectively. Note that the kinetic energy suppression from ref. [149] is not taken into account in the GW power spectra of the figure.

6 Conclusion and discussion

In this paper, holographic bounce solutions, bubble wall velocities and GW power spectra are studied and discussed in holographic dQCD and EW models. For holographic models with first-order phase transitions, holographic bounce solutions can be obtained by setting appropriate boundary conditions. By adding positive and negative perturbations to the bounce solution, the bubble expands or shrinks and the final velocity of the bubble wall can be given. It turns out that the final velocity is still smaller than the speed of sound in the plasma, i.e. the deflagration case, even if the phase transition temperature is very low. Moreover, we find that the critical temperature T_c, temperature at the beginning time of the phase transition $T(t_H)$ and nucleation temperature T_n of the phase transition are close to each other, which makes the holographic bubble fit well with the results of thin-wall approximation. Furthermore, the strength parameter α calculated by the holographic model is about $\alpha \sim 3$ for dQCDPT ($\alpha \sim 0.3$ for EWPT) and the inverse of the duration time β/H is about $\beta/H \sim 10000$, and they are quite different from the weakly coupled field theory results, e.g. refs. [33, 63]. For dQCDPT, the GW power spectrum can reach $10^{-18} - 10^{-19}$ around the peak frequency 0.01 Hz, which cannot be detected by any experiment. For EWPT, the GW power spectrum can reach $10^{-17} - 10^{-20}$ around the peak frequency

JHEP07(2023)225

$1-10$ Hz. For $v_3 \neq 0$ case (Model I), the GW signal is not detectable by any experiment. For $v_6 \neq 0$ case (Model II), it can be detected by Ultimate-DECIGO if the appropriate parameters are chosen.

Referring to the quantum bounce solutions proposed by Coleman and Callan [100, 101] with Neumann boundary condition at the center and Dirichlet boundary condition at the edge, the holographic bounce solution can be yielded. We found that the radius of the critical bubble and the value of condensation at the center reduced with decreasing temperature. If a small positive or negative perturbation is added to the holographic bounce solution, the bubble starts to expand or shrink. Through a long enough evolution, the velocity of the bubble wall reaches a constant value. It turns out that in this holographic model, the bubble velocity is deflagration, i.e., it is less than the speed of sound of the system. Although our calculations are under the probe approximation, that is, without a push to the fluid, the conclusions are similar to the refs. [66–68, 72, 73, 75]. How to get detonation and hybrid cases in the bottom-up model remains an open question.

The radius of the critical bubble and the thickness of the bubble wall can be obtained by the Euclidean action. We found that the bubble radius drops rapidly with decreasing temperature while the wall thickness varies little with temperature. In addition, we find that the critical temperature, temperature at the beginning time of the phase transition and nucleation temperature are close to each other during the holographic phase transition. Therefore the thin-wall approximation is considered to estimate the strength and duration time of the phase transition. It turns out that the more rigorous calculations agree well with the approximation results, verifying the reliability of the approximation.

With the holographic bounce solution and the bubble final velocity, we calculated the GW power spectra of dQCDPT and EWPT. We find that the strength parameter α and the inverse of the duration time β/H calculated by the holographic model differ significantly from the weakly coupled field theory results, which impact the GW signal. The parameter α can reach about 3 for dQCDPT, which is strong phase transition, and about 0.3 for EWPT. The parameter β/H is about 30,000 for dQCDPT and about 10,000 for EWPT, so the holographic phase transition is sufficiently fast. Due to the large parameter β/H, the peak frequency shifts rightward compared to the perturbative field theory results. In addition, the GW spectrum is suppressed due to the small bubble expansion speed. Most importantly, the GW signal is strongly suppressed due to the presence of the factor Υ, making it difficult to be detected by the experiment. Eventually, for dQCDPT, it cannot be detected by any experiment. For EWPT, the signal may be detected by Ultimate-DECIGO only when the appropriate parameters are selected in Model II. Whether it is dQCDPT or EWPT, the FOPT caused by the sextic term has a larger α and smaller β/H and higher GW energy than that caused by the cubic term.

For primordial black holes [158–163], the formula of mechanism [164] cannot be applied because the speed of the bubble at the phase transition is much smaller than the speed of light c. Therefore, it cannot be determined whether the black holes have sufficient probability to be produced. However, since the small bubble wall velocity may lead to a small energy density perturbation during the collision, we can speculate that the primordial black hole is difficult to produce in this holographic model. Also, as in ref. [165], the large parameter β/H is not favorable for the formation of primordial black holes.

JHEP07(2023)225

Acknowledgments

We thank Anping Huang, Mingqiu Li, Jingdong Shao, Dianwei Wang, and Qi-Shu Yan for helpful discussions. We thank Maxim Khlopov, Zhang-Yu Nie, Nicklas Ramberg, Kuver Sinha and Miguel Vanvlasselaer for valuable information. This work is supported by the China Postdoctoral Science Foundation under Grant No. 2021M703169, the Fundamental Research Funds for the Central Universities E2E46303X2, the National Natural Science Foundation of China (NSFC) Grant Nos:12235016, 12221005, 11725523, 11735007, 12275108, and the Strategic Priority Research Program of Chinese Academy of Sciences under Grant Nos XDB34030000 and XDPB15, the start-up funding from University of Chinese Academy of Sciences(UCAS), the Fundamental Research Funds for the Central Universities, and the Guangdong Pearl River Talents Plan under Grant No. 2017GC010480.

References

[1] A. Einstein, *Approximative integration of the field equations of gravitation*, *Sitzungsber. Preuss. Akad. Wiss. Berlin (Math. Phys.)* **1916** (1916) 1.

[2] A. Einstein, *About Gravity Waves*, *Sitzungsber. Preuss. Akad. Wiss. Berlin (Math. Phys.)* (1918) 154.

[3] LIGO Scientific and Virgo collaborations, *Observation of Gravitational Waves from a Binary Black Hole Merger*, *Phys. Rev. Lett.* **116** (2016) 061102 [arXiv:1602.03837] [INSPIRE].

[4] NANOGrav collaboration, *The NANOGrav* 12.5 *yr Data Set: Search for an Isotropic Stochastic Gravitational-wave Background*, *Astrophys. J. Lett.* **905** (2020) L34 [arXiv:2009.04496] [INSPIRE].

[5] LIGO Scientific et al. collaborations, *GWTC-3: Compact Binary Coalescences Observed by LIGO and Virgo During the Second Part of the Third Observing Run*, arXiv:2111.03606 [INSPIRE].

[6] M. Maggiore, *Gravitational Waves. Vol. 1: Theory and Experiments*, Oxford University Press (2007) [DOI:10.1093/acprof:oso/9780198570745.001.0001] [INSPIRE].

[7] R.-G. Cai et al., *The Gravitational-Wave Physics*, *Natl. Sci. Rev.* **4** (2017) 687 [arXiv:1703.00187] [INSPIRE].

[8] M. Maggiore, *Gravitational Waves. Vol. 2: Astrophysics and Cosmology*, Oxford University Press (2018) [DOI:10.1093/oso/9780198570899.001.0001] [INSPIRE].

[9] N. Christensen, *Stochastic Gravitational Wave Backgrounds*, *Rept. Prog. Phys.* **82** (2019) 016903 [arXiv:1811.08797] [INSPIRE].

[10] M. Bailes et al., *Gravitational-wave physics and astronomy in the 2020s and 2030s*, *Nature Rev. Phys.* **3** (2021) 344 [INSPIRE].

[11] LIGO Scientific collaboration, *Advanced LIGO*, *Class. Quant. Grav.* **32** (2015) 074001 [arXiv:1411.4547] [INSPIRE].

JHEP07(2023)225

[12] VIRGO collaboration, *Advanced Virgo: a second-generation interferometric gravitational wave detector*, *Class. Quant. Grav.* **32** (2015) 024001 [arXiv:1408.3978] [INSPIRE].

[13] M. Punturo et al., *The Einstein Telescope: A third-generation gravitational wave observatory*, *Class. Quant. Grav.* **27** (2010) 194002 [INSPIRE].

[14] LIGO SCIENTIFIC collaboration, *Exploring the Sensitivity of Next Generation Gravitational Wave Detectors*, *Class. Quant. Grav.* **34** (2017) 044001 [arXiv:1607.08697] [INSPIRE].

[15] LISA collaboration, *Laser Interferometer Space Antenna*, arXiv:1702.00786 [INSPIRE].

[16] S. Kawamura et al., *The Japanese space gravitational wave antenna DECIGO*, *Class. Quant. Grav.* **23** (2006) S125 [INSPIRE].

[17] H. Kudoh, A. Taruya, T. Hiramatsu and Y. Himemoto, *Detecting a gravitational-wave background with next-generation space interferometers*, *Phys. Rev. D* **73** (2006) 064006 [gr-qc/0511145] [INSPIRE].

[18] G.M. Harry et al., *Laser interferometry for the big bang observer*, *Class. Quant. Grav.* **23** (2006) 4887 [*Erratum ibid.* **23** (2006) 7361] [INSPIRE].

[19] W.-R. Hu and Y.-L. Wu, *The Taiji Program in Space for gravitational wave physics and the nature of gravity*, *Natl. Sci. Rev.* **4** (2017) 685 [INSPIRE].

[20] TIANQIN collaboration, *TianQin: a space-borne gravitational wave detector*, *Class. Quant. Grav.* **33** (2016) 035010 [arXiv:1512.02076] [INSPIRE].

[21] R.N. Manchester et al., *The Parkes Pulsar Timing Array Project*, *Publ. Astron. Soc. Austral.* **30** (2013) 17 [arXiv:1210.6130] [INSPIRE].

[22] M. Kramer and D.J. Champion, *The European Pulsar Timing Array and the Large European Array for Pulsars*, *Class. Quant. Grav.* **30** (2013) 224009 [INSPIRE].

[23] M.A. McLaughlin, *The North American Nanohertz Observatory for Gravitational Waves*, *Class. Quant. Grav.* **30** (2013) 224008 [arXiv:1310.0758] [INSPIRE].

[24] R.N. Manchester, *The International Pulsar Timing Array*, *Class. Quant. Grav.* **30** (2013) 224010 [arXiv:1309.7392] [INSPIRE].

[25] K. Kajantie, M. Laine, K. Rummukainen and M.E. Shaposhnikov, *Is there a hot electroweak phase transition at $m_H \gtrsim m_W$?*, *Phys. Rev. Lett.* **77** (1996) 2887 [hep-ph/9605288] [INSPIRE].

[26] M. Gurtler, E.-M. Ilgenfritz and A. Schiller, *Where the electroweak phase transition ends*, *Phys. Rev. D* **56** (1997) 3888 [hep-lat/9704013] [INSPIRE].

[27] F. Csikor, Z. Fodor and J. Heitger, *Endpoint of the hot electroweak phase transition*, *Phys. Rev. Lett.* **82** (1999) 21 [hep-ph/9809291] [INSPIRE].

[28] Z. Fodor and S.D. Katz, *A New method to study lattice QCD at finite temperature and chemical potential*, *Phys. Lett. B* **534** (2002) 87 [hep-lat/0104001] [INSPIRE].

[29] H.-T. Ding, F. Karsch and S. Mukherjee, *Thermodynamics of strong-interaction matter from Lattice QCD*, *Int. J. Mod. Phys. E* **24** (2015) 1530007 [arXiv:1504.05274] [INSPIRE].

[30] J.M. Cline and P.-A. Lemieux, *Electroweak phase transition in two Higgs doublet models*, *Phys. Rev. D* **55** (1997) 3873 [hep-ph/9609240] [INSPIRE].

[31] P. Basler et al., *Strong First Order Electroweak Phase Transition in the CP-Conserving 2HDM Revisited*, *JHEP* **02** (2017) 121 [arXiv:1612.04086] [INSPIRE].

JHEP07(2023)225

[32] G.C. Dorsch, S.J. Huber, T. Konstandin and J.M. No, *A Second Higgs Doublet in the Early Universe: Baryogenesis and Gravitational Waves*, *JCAP* **05** (2017) 052 [arXiv:1611.05874] [INSPIRE].

[33] M. Li, Q.-S. Yan, Y. Zhang and Z. Zhao, *Prospects of gravitational waves in the minimal left-right symmetric model*, *JHEP* **03** (2021) 267 [arXiv:2012.13686] [INSPIRE].

[34] T. Appelquist, J. Terning and L.C.R. Wijewardhana, *The Zero temperature chiral phase transition in* SU(N) *gauge theories*, *Phys. Rev. Lett.* **77** (1996) 1214 [hep-ph/9602385] [INSPIRE].

[35] F. Sannino and J. Schechter, *Chiral phase transition for* SU(N) *gauge theories via an effective Lagrangian approach*, *Phys. Rev. D* **60** (1999) 056004 [hep-ph/9903359] [INSPIRE].

[36] T. Appelquist, P.S. Rodrigues da Silva and F. Sannino, *Enhanced global symmetries and the chiral phase transition*, *Phys. Rev. D* **60** (1999) 116007 [hep-ph/9906555] [INSPIRE].

[37] J.M. Cline, A.R. Frey and G.D. Moore, *Composite magnetic dark matter and the* 130 *GeV line*, *Phys. Rev. D* **86** (2012) 115013 [arXiv:1208.2685] [INSPIRE].

[38] Y. Bai and P. Schwaller, *Scale of dark QCD*, *Phys. Rev. D* **89** (2014) 063522 [arXiv:1306.4676] [INSPIRE].

[39] G.D. Kribs and E.T. Neil, *Review of strongly-coupled composite dark matter models and lattice simulations*, *Int. J. Mod. Phys. A* **31** (2016) 1643004 [arXiv:1604.04627] [INSPIRE].

[40] J.M. Maldacena, *The Large N limit of superconformal field theories and supergravity*, *Adv. Theor. Math. Phys.* **2** (1998) 231 [hep-th/9711200] [INSPIRE].

[41] S.S. Gubser, I.R. Klebanov and A.M. Polyakov, *Gauge theory correlators from noncritical string theory*, *Phys. Lett. B* **428** (1998) 105 [hep-th/9802109] [INSPIRE].

[42] E. Witten, *Anti-de Sitter space and holography*, *Adv. Theor. Math. Phys.* **2** (1998) 253 [hep-th/9802150] [INSPIRE].

[43] J. Erdmenger, N. Evans, I. Kirsch and E. Threlfall, *Mesons in Gauge/Gravity Duals — A Review*, *Eur. Phys. J. A* **35** (2008) 81 [arXiv:0711.4467] [INSPIRE].

[44] T. Sakai and S. Sugimoto, *Low energy hadron physics in holographic QCD*, *Prog. Theor. Phys.* **113** (2005) 843 [hep-th/0412141] [INSPIRE].

[45] T. Sakai and S. Sugimoto, *More on a holographic dual of QCD*, *Prog. Theor. Phys.* **114** (2005) 1083 [hep-th/0507073] [INSPIRE].

[46] J. Erlich, E. Katz, D.T. Son and M.A. Stephanov, *QCD and a holographic model of hadrons*, *Phys. Rev. Lett.* **95** (2005) 261602 [hep-ph/0501128] [INSPIRE].

[47] A. Karch, E. Katz, D.T. Son and M.A. Stephanov, *Linear confinement and AdS/QCD*, *Phys. Rev. D* **74** (2006) 015005 [hep-ph/0602229] [INSPIRE].

[48] U. Gursoy and E. Kiritsis, *Exploring improved holographic theories for QCD: Part I*, *JHEP* **02** (2008) 032 [arXiv:0707.1324] [INSPIRE].

[49] S.S. Gubser and A. Nellore, *Mimicking the QCD equation of state with a dual black hole*, *Phys. Rev. D* **78** (2008) 086007 [arXiv:0804.0434] [INSPIRE].

[50] J. Grefa et al., *Hot and dense quark-gluon plasma thermodynamics from holographic black holes*, *Phys. Rev. D* **104** (2021) 034002 [arXiv:2102.12042] [INSPIRE].

JHEP07(2023)225

[51] D. Li and M. Huang, *Dynamical holographic QCD model for glueball and light meson spectra*, *JHEP* **11** (2013) 088 [arXiv:1303.6929] [INSPIRE].

[52] Y. Chen, D. Li and M. Huang, *The dynamical holographic QCD method for hadron physics and QCD matter*, *Commun. Theor. Phys.* **74** (2022) 097201 [arXiv:2206.00917] [INSPIRE].

[53] K. Haba, S. Matsuzaki and K. Yamawaki, *S Parameter in the Holographic Walking/Conformal Technicolor*, *Prog. Theor. Phys.* **120** (2008) 691 [arXiv:0804.3668] [INSPIRE].

[54] S. Matsuzaki and K. Yamawaki, *Holographic techni-dilaton at* 125 *GeV*, *Phys. Rev. D* **86** (2012) 115004 [arXiv:1209.2017] [INSPIRE].

[55] D. Elander and M. Piai, *The decay constant of the holographic techni-dilaton and the 125 GeV boson*, *Nucl. Phys. B* **867** (2013) 779 [arXiv:1208.0546] [INSPIRE].

[56] Y. Chen, M. Huang and Q.-S. Yan, *Gravitation waves from QCD and electroweak phase transitions*, *JHEP* **05** (2018) 178 [arXiv:1712.03470] [INSPIRE].

[57] K. Bitaghsir Fadafan, W. Clemens and N. Evans, *Holographic Gauged NJL Model: the Conformal Window and Ideal Walking*, *Phys. Rev. D* **98** (2018) 066015 [arXiv:1807.04548] [INSPIRE].

[58] Y. Chen, X.-J. Bi and M. Huang, *Holographic Technicolor Model and Dark Matter*, *Chin. Phys. C* **44** (2020) 093102 [arXiv:1912.11682] [INSPIRE].

[59] R. Contino, Y. Nomura and A. Pomarol, *Higgs as a holographic pseudoGoldstone boson*, *Nucl. Phys. B* **671** (2003) 148 [hep-ph/0306259] [INSPIRE].

[60] K. Agashe, R. Contino and A. Pomarol, *The Minimal composite Higgs model*, *Nucl. Phys. B* **719** (2005) 165 [hep-ph/0412089] [INSPIRE].

[61] D. Croon, B.M. Dillon, S.J. Huber and V. Sanz, *Exploring holographic Composite Higgs models*, *JHEP* **07** (2016) 072 [arXiv:1510.08482] [INSPIRE].

[62] D. Espriu and A. Katanaeva, *Holographic description of* SO(5) → SO(4) *composite Higgs model*, arXiv:1706.02651 [INSPIRE].

[63] M. Li, Q.-S. Yan and M. Huang, *Anisotropic gravitational waves induced by hypermagnetic fields during the electroweak phase transition epoch*, *Phys. Rev. D* **107** (2023) 043527 [arXiv:2211.03368] [INSPIRE].

[64] M. Attems et al., *Holographic Collisions across a Phase Transition*, *Phys. Rev. Lett.* **121** (2018) 261601 [arXiv:1807.05175] [INSPIRE].

[65] M. Attems et al., *Dynamics of Phase Separation from Holography*, *JHEP* **01** (2020) 106 [arXiv:1905.12544] [INSPIRE].

[66] Y. Bea et al., *Bubble wall velocity from holography*, *Phys. Rev. D* **104** (2021) L121903 [arXiv:2104.05708] [INSPIRE].

[67] Y. Bea et al., *Spinodal Gravitational Waves*, arXiv:2112.15478 [INSPIRE].

[68] F. Bigazzi, A. Caddeo, T. Canneti and A.L. Cotrone, *Bubble wall velocity at strong coupling*, *JHEP* **08** (2021) 090 [arXiv:2104.12817] [INSPIRE].

[69] F. Bigazzi, A. Caddeo, A.L. Cotrone and A. Paredes, *Dark Holograms and Gravitational Waves*, *JHEP* **04** (2021) 094 [arXiv:2011.08757] [INSPIRE].

JHEP07(2023)225

[70] F.R. Ares et al., *Effective actions and bubble nucleation from holography*, *Phys. Rev. D* **105** (2022) 066020 [arXiv:2109.13784] [INSPIRE].

[71] F.R. Ares et al., *Gravitational Waves at Strong Coupling from an Effective Action*, *Phys. Rev. Lett.* **128** (2022) 131101 [arXiv:2110.14442] [INSPIRE].

[72] Y. Bea et al., *Holographic bubbles with Jecco: expanding, collapsing and critical*, *JHEP* **09** (2022) 008 [*Erratum ibid.* **03** (2023) 225] [arXiv:2202.10503] [INSPIRE].

[73] Y. Bea et al., *Domain collisions*, *JHEP* **06** (2022) 025 [arXiv:2111.03355] [INSPIRE].

[74] Q. Chen et al., *Critical dynamics in holographic first-order phase transition*, *JHEP* **01** (2023) 056 [arXiv:2209.12789] [INSPIRE].

[75] R.A. Janik, M. Jarvinen, H. Soltanpanahi and J. Sonnenschein, *Perfect Fluid Hydrodynamic Picture of Domain Wall Velocities at Strong Coupling*, *Phys. Rev. Lett.* **129** (2022) 081601 [arXiv:2205.06274] [INSPIRE].

[76] M. Ahmadvand and K. Bitaghsir Fadafan, *Gravitational waves generated from the cosmological QCD phase transition within AdS/QCD*, *Phys. Lett. B* **772** (2017) 747 [arXiv:1703.02801] [INSPIRE].

[77] M. Ahmadvand and K. Bitaghsir Fadafan, *The cosmic QCD phase transition with dense matter and its gravitational waves from holography*, *Phys. Lett. B* **779** (2018) 1 [arXiv:1707.05068] [INSPIRE].

[78] S. Rezapour, K. Bitaghsir Fadafan and M. Ahmadvand, *Gravitational waves of a first-order QCD phase transition at finite coupling from holography*, *Annals Phys.* **437** (2022) 168731 [arXiv:2006.04265] [INSPIRE].

[79] Z.-R. Zhu, J. Chen and D. Hou, *Gravitational waves from holographic QCD phase transition with gluon condensate*, *Eur. Phys. J. A* **58** (2022) 104 [arXiv:2109.09933] [INSPIRE].

[80] O.O. Novikov and A.A. Shavrin, *Holographic model for the first order phase transition in the composite Higgs scenario*, arXiv:2209.02331 [INSPIRE].

[81] E. Morgante, N. Ramberg and P. Schwaller, *Gravitational waves from dark* SU(3) *Yang-Mills theory*, *Phys. Rev. D* **107** (2023) 036010 [arXiv:2210.11821] [INSPIRE].

[82] K. Chelabi et al., *Realization of chiral symmetry breaking and restoration in holographic QCD*, *Phys. Rev. D* **93** (2016) 101901 [arXiv:1511.02721] [INSPIRE].

[83] K. Chelabi et al., *Chiral Phase Transition in the Soft-Wall Model of AdS/QCD*, *JHEP* **04** (2016) 036 [arXiv:1512.06493] [INSPIRE].

[84] X. Chen, D. Li, D. Hou and M. Huang, *Quarkyonic phase from quenched dynamical holographic QCD model*, *JHEP* **03** (2020) 073 [arXiv:1908.02000] [INSPIRE].

[85] S. Weinberg, *Implications of Dynamical Symmetry Breaking*, *Phys. Rev. D* **13** (1976) 974 [INSPIRE].

[86] L. Susskind, *Dynamics of Spontaneous Symmetry Breaking in the Weinberg-Salam Theory*, *Phys. Rev. D* **20** (1979) 2619 [INSPIRE].

[87] K. Yamawaki, M. Bando and K.-I. Matumoto, *Scale Invariant Technicolor Model and a Technidilaton*, *Phys. Rev. Lett.* **56** (1986) 1335 [INSPIRE].

[88] M. Bando, K.-I. Matumoto and K. Yamawaki, *Technidilaton*, *Phys. Lett. B* **178** (1986) 308 [INSPIRE].

JHEP07(2023)225

[89] M. Bando, T. Morozumi, H. So and K. Yamawaki, *Discriminating technicolor theories through flavor changing neutral currents: Walking or standing coupling constants?*, *Phys. Rev. Lett.* **59** (1987) 389 [INSPIRE].

[90] R. Foadi, M.T. Frandsen, T.A. Ryttov and F. Sannino, *Minimal Walking Technicolor: Set Up for Collider Physics*, *Phys. Rev. D* **76** (2007) 055005 [arXiv:0706.1696] [INSPIRE].

[91] S.B. Gudnason, C. Kouvaris and F. Sannino, *Towards working technicolor: Effective theories and dark matter*, *Phys. Rev. D* **73** (2006) 115003 [hep-ph/0603014] [INSPIRE].

[92] J.M. Cline, M. Jarvinen and F. Sannino, *The Electroweak Phase Transition in Nearly Conformal Technicolor*, *Phys. Rev. D* **78** (2008) 075027 [arXiv:0808.1512] [INSPIRE].

[93] T. Appelquist and G. Triantaphyllou, *Precision tests of technicolor*, *Phys. Lett. B* **278** (1992) 345 [INSPIRE].

[94] R. Sundrum and S.D.H. Hsu, *Walking technicolor and electroweak radiative corrections*, *Nucl. Phys. B* **391** (1993) 127 [hep-ph/9206225] [INSPIRE].

[95] T. Appelquist and F. Sannino, *The Physical spectrum of conformal* SU(N) *gauge theories*, *Phys. Rev. D* **59** (1999) 067702 [hep-ph/9806409] [INSPIRE].

[96] M. Harada, M. Kurachi and K. Yamawaki, *The* $\pi^+ - \pi^0$ *mass difference and the S parameter in large* N_f *QCD*, *Prog. Theor. Phys.* **115** (2006) 765 [hep-ph/0509193] [INSPIRE].

[97] M. Kurachi and R. Shrock, *Behavior of the S Parameter in the Crossover Region Between Walking and QCD-Like Regimes of an* SU(N) *Gauge Theory*, *Phys. Rev. D* **74** (2006) 056003 [hep-ph/0607231] [INSPIRE].

[98] M. Kurachi, R. Shrock and K. Yamawaki, *Z boson propagator correction in technicolor theories with ETC effects included*, *Phys. Rev. D* **76** (2007) 035003 [arXiv:0704.3481] [INSPIRE].

[99] A. Karch, E. Katz, D.T. Son and M.A. Stephanov, *On the sign of the dilaton in the soft wall models*, *JHEP* **04** (2011) 066 [arXiv:1012.4813] [INSPIRE].

[100] S.R. Coleman, *The Fate of the False Vacuum. I. Semiclassical Theory*, *Phys. Rev. D* **15** (1977) 2929 [*Erratum ibid.* **16** (1977) 1248] [INSPIRE].

[101] C.G. Callan Jr. and S.R. Coleman, *The Fate of the False Vacuum. II. First Quantum Corrections*, *Phys. Rev. D* **16** (1977) 1762 [INSPIRE].

[102] A.D. Linde, *Fate of the False Vacuum at Finite Temperature: Theory and Applications*, *Phys. Lett. B* **100** (1981) 37 [INSPIRE].

[103] A.D. Linde, *Decay of the False Vacuum at Finite Temperature*, *Nucl. Phys. B* **216** (1983) 421 [*Erratum ibid.* **223** (1983) 544] [INSPIRE].

[104] O. Gould and J. Hirvonen, *Effective field theory approach to thermal bubble nucleation*, *Phys. Rev. D* **104** (2021) 096015 [arXiv:2108.04377] [INSPIRE].

[105] M.B. Hindmarsh, M. Lüben, J. Lumma and M. Pauly, *Phase transitions in the early universe*, *SciPost Phys. Lect. Notes* **24** (2021) 1 [arXiv:2008.09136] [INSPIRE].

[106] L.N. Trefethen, *Spectral Methods in Matlab*, SIAM: Society for Industrial and Applied Mathematics (2000) [DOI:10.1137/1.9780898719598].

[107] A. Cherman, T.D. Cohen and E.S. Werbos, *The Chiral condensate in holographic models of QCD*, *Phys. Rev. C* **79** (2009) 045203 [arXiv:0804.1096] [INSPIRE].

JHEP07(2023)225

[108] A. Eichhorn et al., *Universal gravitational-wave signatures from heavy new physics in the electroweak sector*, *JCAP* **05** (2021) 006 [arXiv:2010.00017] [INSPIRE].

[109] J.R. Espinosa, T. Konstandin, J.M. No and G. Servant, *Energy Budget of Cosmological First-order Phase Transitions*, *JCAP* **06** (2010) 028 [arXiv:1004.4187] [INSPIRE].

[110] M. Hindmarsh, S.J. Huber, K. Rummukainen and D.J. Weir, *Numerical simulations of acoustically generated gravitational waves at a first order phase transition*, *Phys. Rev. D* **92** (2015) 123009 [arXiv:1504.03291] [INSPIRE].

[111] C. Caprini et al., *Science with the space-based interferometer eLISA. II: Gravitational waves from cosmological phase transitions*, *JCAP* **04** (2016) 001 [arXiv:1512.06239] [INSPIRE].

[112] T. Konstandin and J.M. No, *Hydrodynamic obstruction to bubble expansion*, *JCAP* **02** (2011) 008 [arXiv:1011.3735] [INSPIRE].

[113] M. Barroso Mancha, T. Prokopec and B. Swiezewska, *Field-theoretic derivation of bubble-wall force*, *JHEP* **01** (2021) 070 [arXiv:2005.10875] [INSPIRE].

[114] S. Balaji, M. Spannowsky and C. Tamarit, *Cosmological bubble friction in local equilibrium*, *JCAP* **03** (2021) 051 [arXiv:2010.08013] [INSPIRE].

[115] W.-Y. Ai, B. Garbrecht and C. Tamarit, *Bubble wall velocities in local equilibrium*, *JCAP* **03** (2022) 015 [arXiv:2109.13710] [INSPIRE].

[116] G.D. Moore and T. Prokopec, *How fast can the wall move? A Study of the electroweak phase transition dynamics*, *Phys. Rev. D* **52** (1995) 7182 [hep-ph/9506475] [INSPIRE].

[117] G.D. Moore and T. Prokopec, *Bubble wall velocity in a first order electroweak phase transition*, *Phys. Rev. Lett.* **75** (1995) 777 [hep-ph/9503296] [INSPIRE].

[118] T. Konstandin, G. Nardini and I. Rues, *From Boltzmann equations to steady wall velocities*, *JCAP* **09** (2014) 028 [arXiv:1407.3132] [INSPIRE].

[119] J. Kozaczuk, *Bubble Expansion and the Viability of Singlet-Driven Electroweak Baryogenesis*, *JHEP* **10** (2015) 135 [arXiv:1506.04741] [INSPIRE].

[120] A. Azatov and M. Vanvlasselaer, *Bubble wall velocity: heavy physics effects*, *JCAP* **01** (2021) 058 [arXiv:2010.02590] [INSPIRE].

[121] B. Laurent and J.M. Cline, *Fluid equations for fast-moving electroweak bubble walls*, *Phys. Rev. D* **102** (2020) 063516 [arXiv:2007.10935] [INSPIRE].

[122] G.C. Dorsch, S.J. Huber and T. Konstandin, *A sonic boom in bubble wall friction*, *JCAP* **04** (2022) 010 [arXiv:2112.12548] [INSPIRE].

[123] S. De Curtis et al., *Bubble wall dynamics at the electroweak phase transition*, *JHEP* **03** (2022) 163 [arXiv:2201.08220] [INSPIRE].

[124] B. Laurent and J.M. Cline, *First principles determination of bubble wall velocity*, *Phys. Rev. D* **106** (2022) 023501 [arXiv:2204.13120] [INSPIRE].

[125] A. Adams, P.M. Chesler and H. Liu, *Holographic Vortex Liquids and Superfluid Turbulence*, *Science* **341** (2013) 368 [arXiv:1212.0281] [INSPIRE].

[126] A. Kosowsky, M.S. Turner and R. Watkins, *Gravitational radiation from colliding vacuum bubbles*, *Phys. Rev. D* **45** (1992) 4514 [INSPIRE].

[127] A. Kosowsky, M.S. Turner and R. Watkins, *Gravitational waves from first order cosmological phase transitions*, *Phys. Rev. Lett.* **69** (1992) 2026 [INSPIRE].

JHEP07(2023)225

[128] A. Kosowsky and M.S. Turner, *Gravitational radiation from colliding vacuum bubbles: envelope approximation to many bubble collisions*, *Phys. Rev. D* **47** (1993) 4372 [astro-ph/9211004] [INSPIRE].

[129] M. Kamionkowski, A. Kosowsky and M.S. Turner, *Gravitational radiation from first order phase transitions*, *Phys. Rev. D* **49** (1994) 2837 [astro-ph/9310044] [INSPIRE].

[130] C. Caprini, R. Durrer and G. Servant, *Gravitational wave generation from bubble collisions in first-order phase transitions: An analytic approach*, *Phys. Rev. D* **77** (2008) 124015 [arXiv:0711.2593] [INSPIRE].

[131] S.J. Huber and T. Konstandin, *Gravitational Wave Production by Collisions: More Bubbles*, *JCAP* **09** (2008) 022 [arXiv:0806.1828] [INSPIRE].

[132] C. Caprini, R. Durrer, T. Konstandin and G. Servant, *General Properties of the Gravitational Wave Spectrum from Phase Transitions*, *Phys. Rev. D* **79** (2009) 083519 [arXiv:0901.1661] [INSPIRE].

[133] D.J. Weir, *Revisiting the envelope approximation: gravitational waves from bubble collisions*, *Phys. Rev. D* **93** (2016) 124037 [arXiv:1604.08429] [INSPIRE].

[134] R. Jinno and M. Takimoto, *Gravitational waves from bubble collisions: An analytic derivation*, *Phys. Rev. D* **95** (2017) 024009 [arXiv:1605.01403] [INSPIRE].

[135] M. Hindmarsh, S.J. Huber, K. Rummukainen and D.J. Weir, *Gravitational waves from the sound of a first order phase transition*, *Phys. Rev. Lett.* **112** (2014) 041301 [arXiv:1304.2433] [INSPIRE].

[136] J.T. Giblin Jr. and J.B. Mertens, *Vacuum Bubbles in the Presence of a Relativistic Fluid*, *JHEP* **12** (2013) 042 [arXiv:1310.2948] [INSPIRE].

[137] J.T. Giblin and J.B. Mertens, *Gravitional radiation from first-order phase transitions in the presence of a fluid*, *Phys. Rev. D* **90** (2014) 023532 [arXiv:1405.4005] [INSPIRE].

[138] M. Hindmarsh, S.J. Huber, K. Rummukainen and D.J. Weir, *Shape of the acoustic gravitational wave power spectrum from a first order phase transition*, *Phys. Rev. D* **96** (2017) 103520 [*Erratum ibid.* **101** (2020) 089902] [arXiv:1704.05871] [INSPIRE].

[139] A. Kosowsky, A. Mack and T. Kahniashvili, *Gravitational radiation from cosmological turbulence*, *Phys. Rev. D* **66** (2002) 024030 [astro-ph/0111483] [INSPIRE].

[140] A.D. Dolgov, D. Grasso and A. Nicolis, *Relic backgrounds of gravitational waves from cosmic turbulence*, *Phys. Rev. D* **66** (2002) 103505 [astro-ph/0206461] [INSPIRE].

[141] C. Caprini and R. Durrer, *Gravitational waves from stochastic relativistic sources: Primordial turbulence and magnetic fields*, *Phys. Rev. D* **74** (2006) 063521 [astro-ph/0603476] [INSPIRE].

[142] G. Gogoberidze, T. Kahniashvili and A. Kosowsky, *The Spectrum of Gravitational Radiation from Primordial Turbulence*, *Phys. Rev. D* **76** (2007) 083002 [arXiv:0705.1733] [INSPIRE].

[143] T. Kahniashvili et al., *Gravitational Radiation from Primordial Helical Inverse Cascade MHD Turbulence*, *Phys. Rev. D* **78** (2008) 123006 [*Erratum ibid.* **79** (2009) 109901] [arXiv:0809.1899] [INSPIRE].

[144] T. Kahniashvili, L. Kisslinger and T. Stevens, *Gravitational Radiation Generated by Magnetic Fields in Cosmological Phase Transitions*, *Phys. Rev. D* **81** (2010) 023004 [arXiv:0905.0643] [INSPIRE].

JHEP07(2023)225

[145] C. Caprini, R. Durrer and G. Servant, *The stochastic gravitational wave background from turbulence and magnetic fields generated by a first-order phase transition*, *JCAP* **12** (2009) 024 [arXiv:0909.0622] [INSPIRE].

[146] L. Kisslinger and T. Kahniashvili, *Polarized Gravitational Waves from Cosmological Phase Transitions*, *Phys. Rev. D* **92** (2015) 043006 [arXiv:1505.03680] [INSPIRE].

[147] J. Ellis, M. Lewicki, J.M. No and V. Vaskonen, *Gravitational wave energy budget in strongly supercooled phase transitions*, *JCAP* **06** (2019) 024 [arXiv:1903.09642] [INSPIRE].

[148] T. Alanne, T. Hugle, M. Platscher and K. Schmitz, *A fresh look at the gravitational-wave signal from cosmological phase transitions*, *JHEP* **03** (2020) 004 [arXiv:1909.11356] [INSPIRE].

[149] D. Cutting, M. Hindmarsh and D.J. Weir, *Vorticity, kinetic energy, and suppressed gravitational wave production in strong first order phase transitions*, *Phys. Rev. Lett.* **125** (2020) 021302 [arXiv:1906.00480] [INSPIRE].

[150] H.-K. Guo, K. Sinha, D. Vagie and G. White, *Phase Transitions in an Expanding Universe: Stochastic Gravitational Waves in Standard and Non-Standard Histories*, *JCAP* **01** (2021) 001 [arXiv:2007.08537] [INSPIRE].

[151] J. Ellis, M. Lewicki and J.M. No, *On the Maximal Strength of a First-Order Electroweak Phase Transition and its Gravitational Wave Signal*, *JCAP* **04** (2019) 003 [arXiv:1809.08242] [INSPIRE].

[152] A. Roper Pol et al., *Numerical simulations of gravitational waves from early-universe turbulence*, *Phys. Rev. D* **102** (2020) 083512 [arXiv:1903.08585] [INSPIRE].

[153] P. Auclair et al., *Generation of gravitational waves from freely decaying turbulence*, *JCAP* **09** (2022) 029 [arXiv:2205.02588] [INSPIRE].

[154] P. Niksa, M. Schlederer and G. Sigl, *Gravitational Waves produced by Compressible MHD Turbulence from Cosmological Phase Transitions*, *Class. Quant. Grav.* **35** (2018) 144001 [arXiv:1803.02271] [INSPIRE].

[155] A.H. Guth and S.H.H. Tye, *Phase Transitions and Magnetic Monopole Production in the Very Early Universe*, *Phys. Rev. Lett.* **44** (1980) 631 [*Erratum ibid.* **44** (1980) 963] [INSPIRE].

[156] A.H. Guth and E.J. Weinberg, *Cosmological Consequences of a First Order Phase Transition in the* SU(5) *Grand Unified Model*, *Phys. Rev. D* **23** (1981) 876 [INSPIRE].

[157] M.D. Rintoul and S. Torquato, *Precise determination of the critical threshold and exponents in a three-dimensional continuum percolation model*, *J. Phys. A* **30** (1997) L585.

[158] S. Hawking, *Gravitationally collapsed objects of very low mass*, *Mon. Not. Roy. Astron. Soc.* **152** (1971) 75 [INSPIRE].

[159] B.J. Carr and S.W. Hawking, *Black holes in the early Universe*, *Mon. Not. Roy. Astron. Soc.* **168** (1974) 399 [INSPIRE].

[160] R.V. Konoplich, S.G. Rubin, A.S. Sakharov and M.Y. Khlopov, *Formation of black holes in first-order phase transitions as a cosmological test of symmetry-breaking mechanisms*, *Phys. Atom. Nucl.* **62** (1999) 1593 [INSPIRE].

[161] M.Y. Khlopov, R.V. Konoplich, S.G. Rubin and A.S. Sakharov, *First-order phase transitions as a source of black holes in the early universe*, *Grav. Cosmol.* **6** (2000) 153 [INSPIRE].

JHEP07(2023)225

[162] I. Dymnikova, L. Koziel, M. Khlopov and S. Rubin, *Quasilumps from first order phase transitions*, *Grav. Cosmol.* **6** (2000) 311 [hep-th/0010120] [INSPIRE].

[163] M.Y. Khlopov, *Primordial Black Holes*, *Res. Astron. Astrophys.* **10** (2010) 495 [arXiv:0801.0116] [INSPIRE].

[164] J. Liu et al., *Primordial black hole production during first-order phase transitions*, *Phys. Rev. D* **105** (2022) L021303 [arXiv:2106.05637] [INSPIRE].

[165] J. Shao and M. Huang, *Gravitational waves and primordial black holes from chirality imbalanced QCD first-order phase transition with P and CP violation*, *Phys. Rev. D* **107** (2023) 043011 [arXiv:2209.13809] [INSPIRE].

JHEP07(2023)225